# Detailed electronic structure studies on superconducting $MgB_2$ and related compounds

P. Ravindran,* P. Vajeeston, R. Vidya, A. Kjekshus, and H. Fjellvåg
*Department of Chemistry, University of Oslo, Box 1033, Blindern, N-0315, Oslo, Norway*
(Received 12 April 2001; revised manuscript received 19 July 2001; published 20 November 2001)

In order to understand the unexpected superconducting behavior of $MgB_2$ we have made electronic structure calculations for $MgB_2$ and closely related systems. Our calculated Debye temperature from the elastic properties indicate that the average phonon frequency is very large in $MgB_2$ compared with other superconducting intermetallics and its exceptionally higher $T_c$ can be explained through a BCS mechanism only if phonon softening occurs or the phonon modes are highly anisotropic. We identified a doubly degenerate quasi-two-dimensional key-energy band in the vicinity of $E_F$ along the $\Gamma$–$A$ direction of BZ (having equal amount of B $p_x$ and $p_y$ character) which plays an important role in deciding the superconducting behavior. Based on this result, we have searched for a similar electronic feature in isoelectronic compounds such as $BeB_2$, $CaB_2$, $SrB_2$, LiBC, and $MgB_2C_2$ and found that hole doped LiBC and $MgB_2C_2$ are potential superconducting materials. We have found that $E_F$ in the closely related compound $MgB_4$ is lying in a pseudogap with a negligibly small density of states at $E_F$, which is not favorable for superconductivity. There are contradictory experimental results regarding the anisotropy in the elastic properties of $MgB_2$ ranging from isotropic to moderately anisotropic to highly anisotropic. In order to settle this issue we have calculated the single-crystal elastic constants for $MgB_2$ by the accurate full-potential method and derived the directional-dependent linear compressibility, Young's modulus, shear modulus, and relevant elastic properties from these results. We have observed large anisotropy in the elastic properties consistent with recent high-pressure findings. Our calculated polarized optical dielectric tensor shows highly anisotropic behavior even though it possesses isotropic transport property. $MgB_2$ possesses a mixed bonding character and this has been verified from density of states, charge density, and crystal orbital Hamiltonian population analyses.

DOI: 10.1103/PhysRevB.64.224509 PACS number(s): 74.70.Ad, 74.25.Gz, 74.25.Jb

## I. INTRODUCTION

The recent discovery of superconductivity with higher $T_c$ (Ref. 1) in $MgB_2$ has initiated much activity in experimental as well as theoretical studies. $Nb_3Ge$ has long been the record holder of the highest $T_c$ among the intermetallic superconductors. The recently found $YPd_2B_2C$ touches the same $T_c$ as $Nb_3Ge$. The work of Bednorz and Müller[2] from 1986 on the basis of copper oxides started the discovery of a rapidly increasing number of high-$T_c$ superconductors, among which the current record is held by $HgBa_2Ca_2Cu_3O_{8-\delta}$ with $T_c \approx 164$ K under pressure.[3] During the past decade, remarkable progress in basic research and technological applications has been made on the high-$T_c$ cuprate superconductors. However, the complex crystal structures in combination with the multicomponent nature of the materials involved hinder the full understanding of the microscopic origin of high-$T_c$ superconductivity. Hence, it may be beneficial to study the properties of a simple compound like $MgB_2$ in detail, which does not only have higher $T_c$, but also takes a simple crystal structure with $sp$ electrons (involved in the superconducting process) that are easy to handle theoretically.

The observation of superconductivity with higher $T_c$ in $MgB_2$ raises the question of whether superconductivity with even higher $T_c$ can be found in intermetallics which do not comprise the characteristic $CuO_2$ planes in high-$T_c$ superconductors. Several properties of $MgB_2$ appear closely related to high-$T_c$ superconducting cuprates: a low electron density of states, a layered structural character, and the presence of rather light atoms (like oxygen in cuprates) facilitate high phonon frequencies. Further, although the electronic structure of this material has three-dimensional character, the B–B $\sigma$ bands derived from B $p_x, p_y$ electrons (believed to be important for the superconductivity) reflect two-dimensional character. Like the cuprates, $MgB_2$ appears to exhibit hole conductivity, as evidenced from theoretical considerations[4–7] and experimental Hall coefficient measurement.[8] Another interesting aspect of the $MgB_2$ structure is that it has negatively charged honeycomb-shaped B planes which are reminicent of highly negatively charged Cu–O planes in the high-$T_c$ cuprates.

It is often believed that the $d$ electrons play an important role for the superconducting behavior of intermetallic compounds. So the experimental search for new superconductors has to a large extent been focused on transition-metal compounds. The background for this is that transition-metal compounds usually possess larger density of states (DOS) at the Fermi level than main-group ($sp$) compounds. BCS superconductors usually possess larger DOS at the Fermi level ($E_F$) and the higher $T_c$ in conventional superconductors is related to large $N(E_F)$ values as well as strong coupling of selected phonon modes to the electronic system. Further, the relatively higher $T_c$ in superconducting intermetallics are believed to be coupled to a van Hove-like peak at $E_F$ in the DOS curve, as predicted by various band-structure calculations and indicated experimentally for Ni-site substituted rare-earth nickel borocarbides.[9] In $MgB_2$ there is no such

 

peak-like feature at the vicinity of $E_F$ in the DOS profile. $MgB_2$ is an $sp$ metal and hence its value of $N(E_F)$ is small compared with that of superconducting transition-metal compounds. On the other hand, theoretical studies[7] show that the quasi-two-dimensional B $\sigma$ bands are strongly coupled with $E_{2g}$ phonon modes, which would be consistent with the BCS mechanism. The experimentally observed isotope effect[10] in $MgB_2$ also indicates phonon-mediated superconductivity. The absence of a Hebel–Slichter peak in the nuclear magnetic resonance (NMR) relaxation,[11–14] a temperature-dependent peak around 17 meV in the energy-resolved neutron scattering,[15] a first-order metal-to-metal transition on Al or C substitution,[16–18] apparently anomalous temperature dependencies of the Hall coefficient[19] and London penetration depth,[20] and the need for small $\mu^*$ value to explain the experimentally observed higher $T_c$ by the BCS theory[21] indicate that the mechanism differs significantly from that of the BCS theory.

The discovery of intermetallic superconductors like borocarbides[22,23] and boronitrides[24] with relatively higher $T_c$ [up to 23 K for $YPd_2B_2C$ (Ref. 23)], has encouraged the search for superconductivity in materials possessing light atoms such as B, C, N, H, etc. Superconductivity with $T_c$ in the range 2–4 K has been observed for ternary transition-metal diborides ($YRe_2B_2$, $LuB_2C_2$, $YB_2C_2$)[25,26] and in magnetic rare-earth (RE) rhodium borides [$RERh_4B_4$ (Ref. 27)]. Very recently, the layer-structure compounds $\beta$-ZrNCl and $\beta$-HfNCl ($T_c = 25.5$ K) have been found to be superconducting upon Li intercalation.[28] Another group of materials (maximum $T_c = 9.97$ K reported[29] for $Y_2C_2I_2$) is RE carbide halide superconductors with C–C pairs located in octahedrally coordinated voids of close-packed RE atoms. The recent discovery of superconductivity[30] at $\sim 14$ K in the $AlB_2$-type phase $CaSi_2$ indicates that the $AlB_2$-type structure may be favorable for superconductivity.

There are several mechanisms proposed for the higher $T_c$ in $MgB_2$ and the like. One is based on band-structure findings,[4,21] which suggests that the superconducting state results from strong electron–phonon interaction and high-phonon frequency associated with the light boron atom. This is supported by the relatively large boron isotope effect on $T_c$.[10] Experimentally observed[31] decrease in $T_c$ with pressure at a rate of $-1.11$ K/GPa is consistent with the BCS framework. The low mass of boron is suggested to be conducive to the occurrence of high-phonon frequencies and consequently for higher $T_c$. Another mechanism called the ''universal,''[5] conjectures that the superconductivity in $MgB_2$ (similar to that in cuprate superconductors) is driven by the pairing of the heavily dressed holes in bands that are almost full to gain enough kinetic energy to overcome the Coulomb repulsion. A positive pressure effect on $T_c$ has also been predicted[5] when the pressure reduces the interatomic B–B distance. An and Pickett[7] maintain that the B $\sigma$ bands are playing an important role in the superconductivity of $MgB_2$, and that the B in-plane $E_{2g}$ phonon mode is strongly coupled to this band. Contradictory to the above-mentioned viewpoint, Baskaran[11] concluded from the resonance-valence-bond (RVB) theory that the two-dimensional $\sigma$ bands do not play a crucial role in establishing higher $T_c$ superconductivity and the $p\pi$ band might interfere with superconductivity.

From high-pressure total-energy studies Loa and Syassen[32] concluded that $MgB_2$ has isotropic compressibility. From a high-resolution x-ray powder diffraction high-pressure study along with density functional calculations, Vogt *et al.*[33] concluded that $MgB_2$ possesses nearly isotropic mechanical behavior. From isothermal compressibility measurements Prassides[34] concluded that $MgB_2$ is a stiff tightly packed incompressible solid with only moderate bonding anisotropy between inter- and intralayer directions. However, Jorgensen *et al.*[35] found unusually large anisotropy in thermal expansion and compressibility. So, it is interesting to calculate the single-crystal elastic constants of $MgB_2$ to identify the exact nature of the anisotropy.

Several attempts have been made to enhance $T_c$ by substitution of such elements as Al,[16] Be,[36] Zn,[37] and Li,[38] for Mg and C (Ref. 17) for B, but no practical progress has hitherto been obtained. Moreover, the role of Mg and B site substitution on the electronic structure of $MgB_2$ has been studied theoretically.[39] So, it is interesting to search for compounds with an electronic structure similar to that of $MgB_2$. Knowledge of electronic structure, DOS, Debye temperature, and related properties are important for assessing the mechanism and nature of superconductivity. In a search for superconducting diborides, $BeB_2$ is a promising candidate since the lighter Be may help to provide larger phonon frequencies and hence increase $T_c$. If the electron per atom ratio is important for the superconductivity in this class, one should also consider $CaB_2$ and $SrB_2$ as interesting candidates. If it is the combination of Mg and B which brings the superconductivity in $MgB_2$, one has to consider $MgB_4$ also. If the number of electrons in the B layers is a key for superconductivity in $MgB_2$, attention should be paid to related layer-structured materials such as LiBC and $MgB_2C_2$. For these reasons we have made detailed electronic structure studies for the above-mentioned compounds.

The rest of the paper is organized as follows. The structural aspects and the computational details about the calculations of the electronic structure, optical spectra, and elastic constants are given in Sec. II. In Sec. III we have analyzed the bonding behavior of $MgB_2$ using the orbital and site projected DOS, crystal orbital overlap Hamiltonian population (COHP), charge density analysis, etc. The electronic band structure of $MgB_2$ is calculated and compared with that of closely related systems and also analyzed for possible connections between electronic structure and superconductivity. The elastic and optical anisotropies of this material are calculated and compared with available experimental results. Important findings are summarized in Sec. IV.

## II. STRUCTURAL ASPECTS AND COMPUTATIONAL DETAILS

### A. Crystal structure details

$MgB_2$ [Fig. 1(a)] has the $AlB_2$-type structure[40] with space group $P6/mmm$ and lattice parameters, $a = 3.084$ and $c$

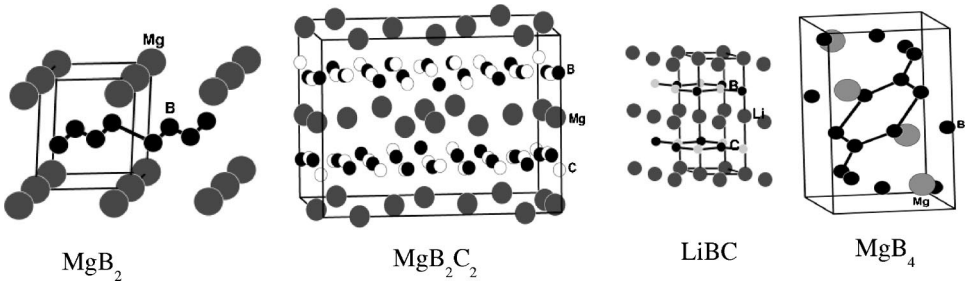


FIG. 1. Crystal structures of $MgB_2$, $MgB_2C_2$, LiBC, and $MgB_4$. Legends to the different kinds of atoms are given in the illustration.

$=3.522$ Å. It is a simple hexagonal lattice of close-packed Mg layers alternating with graphite-like B layers, viz. B atoms arranged at the corners of a hexagon with three nearest-neighbor B atoms in each plane. The Mg atoms are located at the center of the B hexagon, midway between adjacent B layers.

$MgB_2C_2$ crystallizes in an orthorhombic structure,[41] space group $Cmca$ with $a=10.92$, $b=9.46$, and $c=7.45$ Å. The structure of $MgB_2C_2$ [Fig. 1(b)] contains graphite-like but slightly puckered boron–carbon layers whose charge is counterbalanced by "$Mg^{2+}$" cations. The mutual coordination of boron and carbon consists of five atoms of the other kind, three of which are located in the same and two in adjacent layers. Each of Mg is coordinated to six B and six C atoms arranged at the corners of a slightly distorted hexagonal prism. The B–C distances within the layers range from 1.562 to 1.595 Å.

LiBC [Fig. 1(c)] crystallizes[42] in a hexagonal primitive lattice with space group $P6_3/mmc$. The lattice parameters are $a=2.752$ and $c=7.058$ Å. The B and C atoms form a planar so-called heterographite layer. The interlayer regions are filled by Li. The B–C distance of 1.589 Å in LiBC is comparable with that in $MgB_2C_2$.

In $MgB_4$, the B atoms form interconnected pentagonal pyramids with the Mg atoms located in channels running parallel to the $c$ axis. The Mg atoms form zig-zag chains. $MgB_4$ is orthorhombic, space group $Pnma$, with $a=5.46$, $b=7.47$, and $c=4.42$ Å.[43] The average B–B distance in the pentagonal pyramid is 1.787 Å.

Whenever possible we have used the experimental lattice paramenters for our calculation, whereas for $BeB_2$, $CaB_2$, and $SrB_2$ we have used the optimized structural parameters obtained from total-energy minimization.

### B. Computational details for the full-potential linearized-augmented plane wave calculations

These investigations are based on *ab initio* electronic structure calculations derived from density-functional theory. For the screened plasma frequency and the orbital projected DOS calculations we have applied the full-potential linearized-augmented plane wave (FPLAPW) method[44] in a scalar-relativistic version without spin-orbit (SO) coupling. In the calculation we have used atomic sphere radii 1.8 and 1.5 a.u. for Mg and B, respectively. The charge density and the potentials are expanded into lattice harmonics up to $l=6$ inside the spheres and into a Fourier series in the interstitial region. The initial basis set included $3s$, $3p$, and $3d$ valence and $2s$, $2p$ semicore functions at the Mg site, $2s$, $2p$, and $3d$ valence functions for the B site. The set of basis functions was supplemented with local orbitals for additional flexibility in representing the semicore states and for relaxing the linearization errors generally. The effects of exchange and correlation are treated within the generalized-gradient-corrected local-density approximation using the parametrization scheme of Perdew, Burke, and Ernzerhof.[45] To ensure convergence for the Brillouin zone (BZ) integration, 320 **k** points in the irreducible wedge of the first BZ of the hexagonal lattice for $MgB_2$ were used. Self-consistency was achieved by demanding the convergence of the total energy to be smaller than $10^{-5}$ Ry/cell. This corresponds to a convergence of the charge below $10^{-4}$ electrons/atom. For $BeB_2$, $CaB_2$, and $SrB_2$ we have made the structural optimization with a similar procedure.

### C. Computational details for the TB-LMTO calculations

To calculate the electronic ground state properties of $MgB_4$, $MgB_2C_2$, and LiBC we used the TB-LMTO method of Andersen.[46] The von Barth–Hedin parametrization is used for the exchange correlation potential within the local-density approximation. In the present calculation, we used atomic sphere approximation. The calculations are semirelativistic, i.e., without spin-orbit coupling, all other relativistic effects are included, also taking into account combined correction terms. BZ **k**-point integrations are made using the tetrahedron method on a grid of 405 ($MgB_4$), 365 ($MgB_2C_2$) and 549 (LiBC) **k** points in the irreducible part of BZ. In order to have more insight into the chemical bonding, we have also evaluated the crystal orbital Hamiltonian population (COHP)[47,48] in addition to the regular band-structure calculations. COHP is DOS weighted by the corresponding Hamiltonial matrix elements, a positive sign of which indicates bonding character and negative antibonding character.

### D. Computational details of FPLMTO calculations

The full-potential LMTO[49] calculations presented in this paper are all electron, and no shape approximation to the charge density or potential has been used. The base geometry in this computational method consists of muffin-tin and interstitial parts. The basis set is comprised of augmented linear muffin-tin orbitals.[50] Inside the muffin-tin spheres the basis functions, charge density, and potential are expanded in symmetry adapted spherical harmonic functions together with a radial function. Fourier series are used in the interstitial regions. In the present calculations the spherical-harmonic expansion of the charge density, potential, and ba-

sis functions was carried out up to $\ell = 6$. The tails of the basis functions outside their parent spheres are linear combinations of Hankel or Neumann functions depending on the sign of the kinetic energy of the basis function in the interstitial regions. For the core-charge density, the Dirac equation is solved self-consistently, i.e., no frozen core approximation is used. The calculations are based on the generalized-gradient-corrected-density-functional theory as proposed by Perdew, Burke, and Ernzerhof.[45] SO terms are included directly in the Hamiltonian matrix elements for the part inside the muffin-tin spheres. Moreover, the present calculations make use of a so-called multibasis, to ensure a well-converged wave function. This means that we use different Hankel or Neuman functions each attaching to its own radial function. This is important to obtain a reliable description of the higher lying unoccupied states, especially for the optical property studies. For our elastic properties study we have used 192 **k** points and for the optical property studies 624 **k** points in the irreducible part of BZ.

### E. Calculation of optical properties

Once the energies $\epsilon_{\mathbf{k}n}$ and functions $|\mathbf{k}n\rangle$ for the $n$ bands are obtained self consistently, the interband contribution to the imaginary part of the dielectric functions $\epsilon_2(\omega)$ can be calculated by summing the transitions from occupied to unoccupied states (with fixed **k** vector) over BZ, weighted with the appropriate matrix element for the probability of the transition. To be specific, the components of $\epsilon_2(\omega)$ are given by

$$\epsilon_2^{ij}(\omega) = \frac{Ve^2}{2\pi\hbar m^2\omega^2}\int d^3k \sum_{nn'} \langle \mathbf{k}n|p_i|\mathbf{k}n'\rangle\langle \mathbf{k}n'|p_j|\mathbf{k}n\rangle \times f_{\mathbf{k}n}(1-f_{\mathbf{k}n'})\,\delta(\epsilon_{\mathbf{k}n'}-\epsilon_{\mathbf{k}n}-\hbar\omega), \quad (1)$$

where $(p_x, p_y, p_z) = \mathbf{p}$ is the momentum operator and $f_{\mathbf{k}n}$ is the Fermi distribution. The evaluation of matrix elements in Eq. (1) is done over the muffin-tin and interstitial regions separately. Further details about the evaluation of matrix elements are given elsewhere.[51] For the hexagonal structure of $MgB_2$ the dielectric function is a tensor. By an appropriate choice of the principal axes we can diagonalize it and restrict our consideration to the diagonal matrix elements. We have calculated the two components $E\|a$ and $E\|c$ of the dielectric constants corresponding to the electric field parallel to the crystallographic axes $a$ and $c$, respectively. These calculations yield the unbroadened functions. To reproduce the experimental conditions correctly, it is necessary to broaden the calculated spectra. The exact form of the broadening function is unknown, although comparison with measurements suggests that the broadening usually increases with increasing excitation energy. Also the instrumental resolution smears out many fine features. To simulate these effects the lifetime broadening was simulated by convoluting the absorptive part of the dielectric function with a Lorentzian, whose full width at half maximum (FWHM) is equal to $0.01(\hbar\omega)^2$. The experimental resolution was simulated by broadening the final spectra with a Gaussian, where FWHM is equal to 0.02 eV. For metals, the intraband contribution to the optical dielectric tensor influences the lower-energy part of the spectra. This has been calculated using the screened plasma frequency obtained from Fermi surface integration according to the description in Ref. 52.

### F. Calculation of elastic properties

For the single-crystal elastic constant calculations we have adopted the same approach we used earlier[53] for orthorhombic $TiSi_2$. The hexagonal phase of $MgB_2$ has two lattice parameters $a$ and $c$ with Bravais lattice vectors in matrix form

$$\mathbf{R} = \begin{pmatrix} \frac{\sqrt{3}}{2} & \frac{-1}{2} & 0 \\ 0 & 1 & 0 \\ 0 & 0 & \frac{c}{a} \end{pmatrix}.$$

The FPLMTO[49] method allows total-energy calculations to be done for arbitrary crystal structures. We can therefore apply small strains to the equilibrium lattice, then determine the resulting change in the total energy, and from this information deduce the elastic constants. The elastic constants are identified as proportional to the second-order coefficient in a polynomial fit of the total energy as a function of the distortion parameter $\delta$.[54] We determine linear combinations of the elastic constants by straining the lattice vectors **R** according to the relation $\mathbf{R}' = \mathbf{RD}$. Here $\mathbf{R}'$ is a matrix containing the components of the distorted lattice vectors and **D** the symmetric distortion matrix, which contains the strain components. We shall consider only small lattice distortions in order to remain within the elastic limit of the crystal. In the following we shall briefly list the relevant formulae used to obtain the elastic constants for hexagonal crystals. The internal energy of a crystal under strain, $\delta$, can be Taylor expanded in powers of the strain tensor with respect to the initial internal energy of the unstrained crystal in the following way:

$$E(V,\delta) = E(V_0,0) + V_0\left(\sum_i \tau_i\xi_i\delta_i + 1/2\sum_{ij} c_{ij}\delta_i\xi_i\delta_j\xi_j\right) + O(\delta^3). \quad (2)$$

The volume of the unstrained system is denoted $V_0$, $E(V_0,0)$ being the corresponding total energy. In Eq. (2), $\tau_i$ is an element in the stress tensor.

Since we have five independent elastic constants, we need five different strains to determine them. The five distortions used in the present investigation are described in the following. The first distortion

$$D_1 = \begin{pmatrix} 1+\delta & 0 & 0 \\ 0 & 1+\delta & 0 \\ 0 & 0 & 1+\delta \end{pmatrix}$$

gives compression or expansion to the system. This preserves the symmetry but changes the volume. The strain energy associated with this distortion is

$$E(V,\delta)=E(V_0,0)+V_0[(\tau_1+\tau_2+\tau_3)\delta+\tfrac{1}{2}(2c_{11}+2c_{12}+4c_{13}+c_{33})\delta^2].$$

The second distortion

$$D_2=\begin{pmatrix}(1+\delta)^{-1/3} & 0 & 0\\ 0 & (1+\delta)^{-1/3} & 0\\ 0 & 0 & (1+\delta)^{2/3}\end{pmatrix}$$

gives the volume- and symmetry-conserving variation of $c/a$. The energy associated with this distortion is

$$E(V,\delta)=E(V_0,0)+V_0[(\tau_1+\tau_2+\tau_3)\delta+\tfrac{1}{9}(c_{11}+c_{12}-4c_{13}+2c_{33})\delta^2].$$

The strain matrix

$$D_3=\begin{pmatrix}\dfrac{1+\delta}{(1-\delta^2)^{1/3}} & 0 & 0\\ 0 & \dfrac{1-\delta}{(1-\delta^2)^{1/3}} & 0\\ 0 & 0 & \dfrac{1}{(1-\delta^2)^{1/3}}\end{pmatrix}$$

distorts the basal plane by elongation along $a$ and compression along $b$ in such a way that the volume is conserved. The energy associated with this distortion is

$$E(V,\delta)=E(V_0,0)+V_0[(\tau_1-\tau_2)\delta+(c_{11}-c_{12})\delta^2].$$

The elastic constant $c_{55}$ can be determined by the distortion of the lattice using the volume-conserving triclinic distortion

$$D_4=\begin{pmatrix}\dfrac{1}{(1-\delta^2)^{1/3}} & 0 & \dfrac{\delta}{(1-\delta^2)^{1/3}}\\ 0 & \dfrac{1}{(1-\delta^2)^{1/3}} & 0\\ \dfrac{\delta}{(1-\delta^2)^{1/3}} & 0 & \dfrac{1}{(1-\delta^2)^{1/3}}\end{pmatrix}.$$

The energy change associated with this distortion is

$$E(V,\delta)=E(V_0,0)+V_0[\tau_5\delta+(2c_{55})\delta^2].$$

The fifth strain

$$D_5=\begin{pmatrix}1 & 0 & 0\\ 0 & 1 & 0\\ 0 & 0 & 1+\delta\end{pmatrix}$$

involves stretching of the $c$ axis while keeping other axes unchanged. Hence, the hexagonal symmetry is preserved, but volume is changed. The energy change associated with this strain can be written as

$$E(V,\delta)=E(V_0,0)+V_0\left[\tau_3\delta+\left(\frac{c_{33}}{2}\right)\delta^2\right].$$

The elastic constant $c_{33}$ can be directly obtained from the above-mentioned relation. By solving the linear equations given previously we have obtained all five elastic constants. From pressure-dependent lattice parameter measurements it is easy to obtain the bulk modulus along the crystallographic axes. Also to quantify the mechanical anisotropy of $MgB_2$ it is important to calculate the bulk modulus along the axes. For hexagonal crystals the bulk modulus along $a$ ($B_a$) and $c$ ($B_c$) are defined as

$$B_a=a\frac{dP}{da}=\frac{\Lambda}{2+\alpha}$$

and

$$B_c=c\frac{dP}{dc}=\frac{B_a}{\alpha},$$

where $\Lambda=2(c_{11}+c_{12})+4c_{13}\alpha+c_{33}\alpha^2$ and

$$\alpha=\frac{c_{11}+c_{12}-2c_{13}}{c_{33}-c_{13}}.$$

The calculated bulk modulus along the crystallographic axes obtained from these relations are compared with the experimental results in Sec. III.

## III. RESULTS AND DISCUSSION

### A. Electronic structure

An interesting feature of the calculated electronic band structure of $MgB_2$ is that doubly degenerate, nearly flat bands are present just above $E_F$ in the $\Gamma$–$A$ direction (Fig. 2) and cut $E_F$ along the $K$–$\Gamma$ direction. These bands give rise to nearly cylindrical, hole-like Fermi surfaces around the $\Gamma$ point,[4] indicating that the transport properties are dominated by the hole carriers in the plane where B atoms exist. These bands are incompletely filled bonding $\sigma$ bands with predominantly boron $p_x$,$p_y$ character. The $p_z$ bands (mainly in the unoccupied state and with finite contribution along the $M$–$\Gamma$ direction of VB in Fig. 2) are derived from the intralayer $\pi$ bonding orbitals which also have interlayer couplings between adjacent atomic orbitals in the $c$ direction. Our earlier study[55] on superconducting $La_3X$ (X=Al,Ga, In, Tl) compounds show that the presence of a flat band in the vicinity of $E_F$ gives large $T_c$. The flat-band feature is also present in the recently discovered superconducting compound

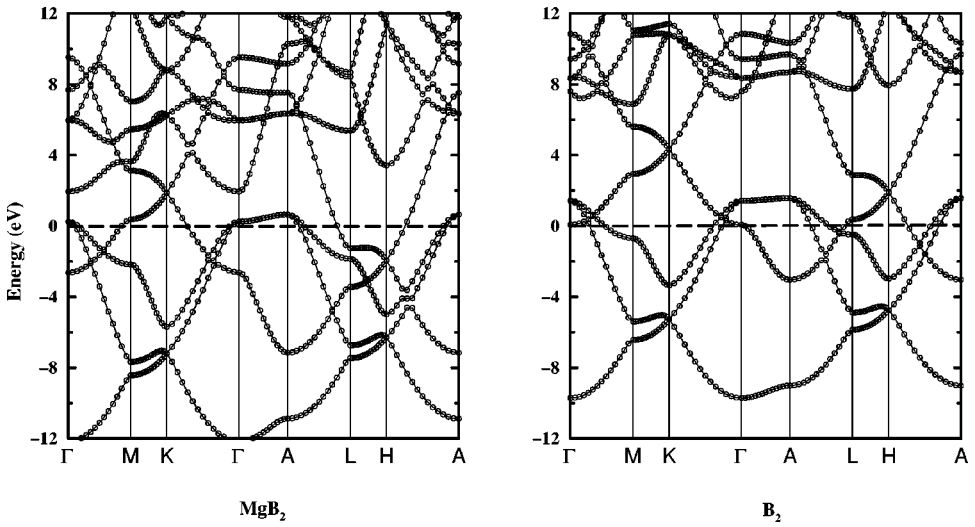


FIG. 2. Band structure of $MgB_2$ and hypothetical $B_2$ in the $AlB_2$-type framework. For the $B_2$ substructure we have used the lattice parameters of $MgB_2$.

$YNi_2B_2C$. As a working hypothesis, we suggest that this flat-band feature plays an important role for the superconductivity in $MgB_2$. The calculated[21] electron–phonon interaction strength also shows a large value in the $\Gamma$–$A$ direction where the flat-band feature is seen. Moreover, zone boundary phonon calculations show that this band feature is very sensitive to the $E_{2g}$ mode (B-bond stretching). The top of this flat-band feature is around 0.54 eV above $E_F$. Assuming rigid-band filling the addition of $\sim$0.32 electron to $MgB_2$ will bring $E_F$ to the top of this energy band. Thus, if electrons are responsible for the superconductivity one can expect enhancement of $T_c$ on electron doping. The electron doping[16] in $Mg_{1-x}Al_xB_2$ leads to a smooth drop in $T_c$ up to $x=0.1$ and beyond $x=0.25$ the superconductivity is completely destroyed. This indicates that holes are responsible for the superconductivity in $MgB_2$, an observation consistent with Hall effect measurements.[8]

The role of Mg on the band structure of $MgB_2$ can be elucidated by completely removing the Mg atoms from the lattice and repeating the calculations for a hypothetical structure with only B atoms (note: using the lattice parameters for $MgB_2$). The calculated electronic structure for the B network alone is given in Fig. 2 along with that of $MgB_2$. The striking difference between the two cases is in the position of the flat band in the $\Gamma$–$A$ direction. This flat-band feature for the B network alone is strongly two dimensional (viz. very little dispersion along $\Gamma$–$A$). This is $\sim$1.8 eV above $E_F$ owing to the smaller number of electrons in the B network compared with $MgB_2$. This suggests that the B–B $\sigma$ bonds are primarily responsible for the superconductivity in $MgB_2$. Interestingly the bands are not deformed appreciably when we remove Mg from $MgB_2$ indicating that the electrons from Mg atoms mainly give a shift in $E_F$ almost like rigid-band filling. This viewpoint is confirmed also from the density of states (Fig. 3), which shows that the topology of the DOS profile with and without Mg atoms in $MgB_2$ are almost the same. But a shift in DOS is observed when Mg is removed from $MgB_2$.

$BeB_2$ could be expected to have a higher $T_c$ owing to the lighter Be atoms which may provide larger phonon frequencies while maintaining a similar electronic structure to that of $MgB_2$. Even though $BeB_2$ is isoelectronic with $MgB_2$, a recent experimental study[36] did not reveal any sign of superconductivity down to 5 K. This negative finding makes it interesting to investigate the electronic structure of $BeB_2$ in detail. The lattice constants for $BeB_2$ obtained[56] by averag-

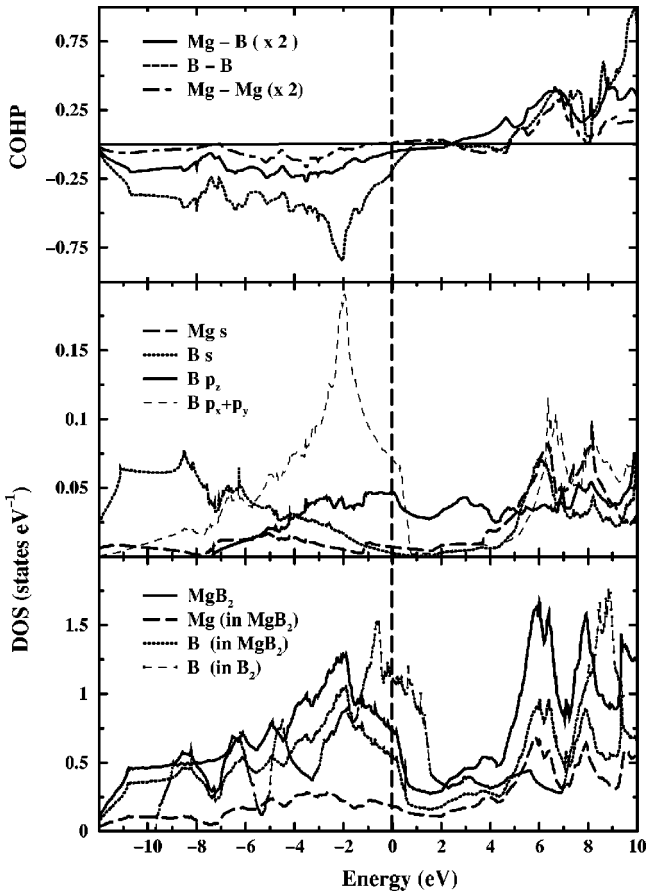


FIG. 3. Lower panel: Total and site-projected DOS for $MgB_2$ and hypothetical $B_2$ obtained from the FPLMTO method. Middle panel: Angular momentum- and orbital-projected DOS for $MgB_2$ obtained from the FPLAPW method. Upper panel: Crystal overlap Hamiltonian population (COHP) between Mg–Mg, Mg–B, and B–B obtained from the TBLMTO method.

TABLE I. Calculated lattice parameters ($a$ and $c$ are in Å), $c/a$ ratio, bulk modulus ($B_0$ in Mbar), its pressure derivative ($B_0'$), and density of states at the Fermi level [$N(E_F)$ in states $Ry^{-1}$ f.u.$^{-1}$] for $AlB_2$-type compounds.

| Compound | $a$ | $c$ | $c/a$ | $B_0$ | $B_0'$ | $N(E_F)$ |
|---|---|---|---|---|---|---|
| $BeB_2$ | 2.886 | 3.088 | 1.027 | 1.93 | 3.47 | 6.309 |
| $MgB_2$ | 3.080 | 3.532 | 1.147 | 1.50 | 3.50 | 9.98 |
| | | | | $1.20\pm0.05$[a] | | |
| | | | | 1.51[b] | | |
| | | | | 1.39[c] | | |
| | | | | 1.47[d] | | |
| | | | | $1.40\pm0.06$[e] | | |
| $CaB_2$ | 3.397 | 4.019 | 1.183 | 1.34 | 3.42 | 10.837 |
| $SrB_2$ | 3.456 | 4.193 | 1.213 | 1.05 | 2.28 | 4.732 |
| $TiB_2$ | 3.070 | 3.262 | 1.060 | 2.13 | 2.10 | 4.27 |

[a]From synchrotron XRD by Prassides *et al.* (Ref. 34).
[b]High-pressure XRD measurement by Vogt *et al.* (Ref. 33).
[c]Calculated from FPLAPW method by Vogt *et al.* (Ref. 33).
[d]Calculated from pseudopotential method by Bohnen *et al.* (Ref. 84).
[e]Calculated from FPLAPW method by Lao and Syassen (Ref. 32).

ing experimental data for the actual unit cell have been inferred to be $a=2.94$ and $c=2.87$ Å. There are no experimental lattice parameters available for $BeB_2$ with the $AlB_2$-type structure and hence we have made structural optimization using the FPLAPW method. Table I shows that $a$ would be reduced by about 6.5%, and $c$ by about 12.5% when Mg is replaced by Be. The anisotropic changes of the lattice parameters can be understood from the anisotropic bonding situation in $MgB_2$. It looks as if the strong B $(p-p)$ $\sigma$ bonds within the planes prevent more appreciable changes in $a$ whereas the weaker $\pi$ bonds along with the relatively weak ionic bonding between Be and B bring about a larger change in $c$. Consistent with the earlier calculation[57] our value of DOS at $E_F$ for $BeB_2$ is smaller than that of $MgB_2$. Owing to the smaller volume our calculated bulk modulus for $BeB_2$ becomes larger than that of $MgB_2$ (Table I).

The total DOS curve for $BeB_2$ (Fig. 4) shows almost free-electron-like metallic feature, with an $N(E_F)$ value of 6.309 state $Ry^{-1}$ f.u.$^{-1}$, which in turn is consistent with the paramagnetic behavior observed experimentally. The DOS curves of $BeB_2$ and $MgB_2$ are indeed very similar as expected due to their isoelectronic and postulated isostructural nature. As mentioned previously, the DOS features could lead one to a higher $T_c$ for $BeB_2$ than for $MgB_2$. A closer inspection of the band structure (Fig. 5) indicates that the key energy band, which we believe to be responsible for superconductivity, is broader in $BeB_2$ than in $MgB_2$ and it is also located well above $E_F$. Hence the calculations suggest that even if one could stabilize $BeB_2$ in the $AlB_2$-type structure one should not expect superconductivity. This conclusion is consistent with the experimental observation in the sense that a recent study[36] shows paramagnetic behavior down to 5 K.

Kortus *et al.*[4] suggested that Ca doping should lead to an overall increase in DOS, and also provide an additional contribution to the electron–phonon coupling. We have therefore

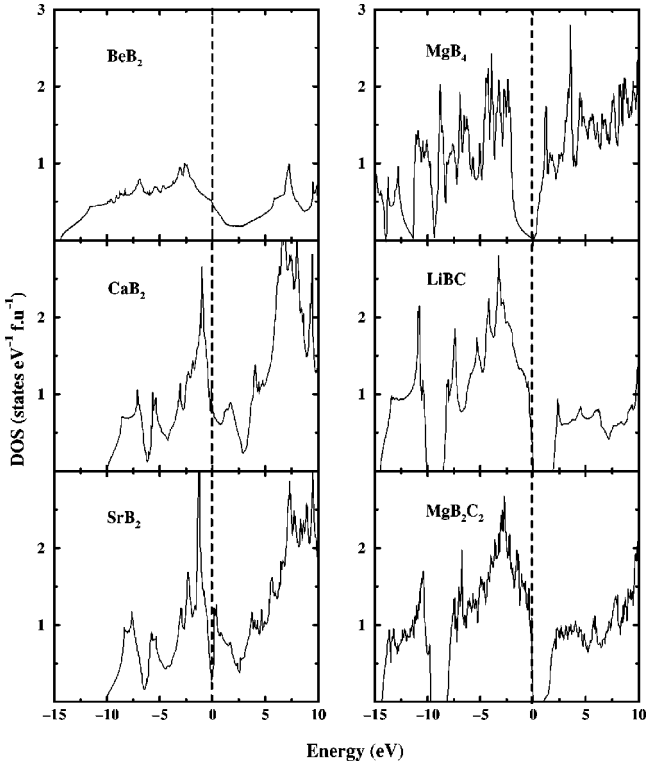


FIG. 4. Calculated total DOS for $BeB_2$, $CaB_2$, and $SrB_2$ obtained from the FPLAPW method and that for $MgB_4$, LiBC, and $MgB_2C_2$ obtained from the TBLMTO method. For $BeB_2$, $CaB_2$, and $SrB_2$ we have assumed the $AlB_2$-type structure and optimized the structural parameters.

calculated DOS (using the optimized structural parameters) for $CaB_2$ which shows (Fig. 4) sharp features like those found in transition metal phases resulting from enhancement in volume compared with $MgB_2$. Also, the calculated DOS at $E_F$ is larger than that of $MgB_2$ indicating a possibility for superconductivity. The larger volume compared with $BeB_2$ and $MgB_2$ along with the weak B–B interaction make the bulk modulus for this material become smaller. The electronic structure of $CaB_2$ (Fig. 5) shows that the key energy band is broader than that in $MgB_2$. Also this doubly degenerate band is well below $E_F$ at the $\Gamma$ point and well above $E_F$ at the $A$ point. Hence, the calculations suggest that the probability for superconductivity in $CaB_2$ with $AlB_2$-type structure is low.

The total DOS for $SrB_2$ (Fig. 4) predicts a pseudogap feature at $E_F$ (separating bonding from antibonding states with a negligible DOS at $E_F$). The electronic structure of $SrB_2$ (Fig. 5) shows nearly semimetallic feature. Earlier studies[58,59] indicate that materials with $E_F$ located at a pseudogap in DOS will have relatively high stability (the situation with all bonding orbitals filled and all antibonding orbitals empty implies extra contribution to stability). Hence the calculations predict that $SrB_2$ with $AlB_2$-type structure may be stabilized experimentally if the above-mentioned criterion works. However, materials with $E_F$ located in the pseudogap are not expected to become superconducting[55] and hence the present finding suggests that $SrB_2$ should be nonsuperconducting. Compared to $BeB_2$ and $MgB_2$, the top

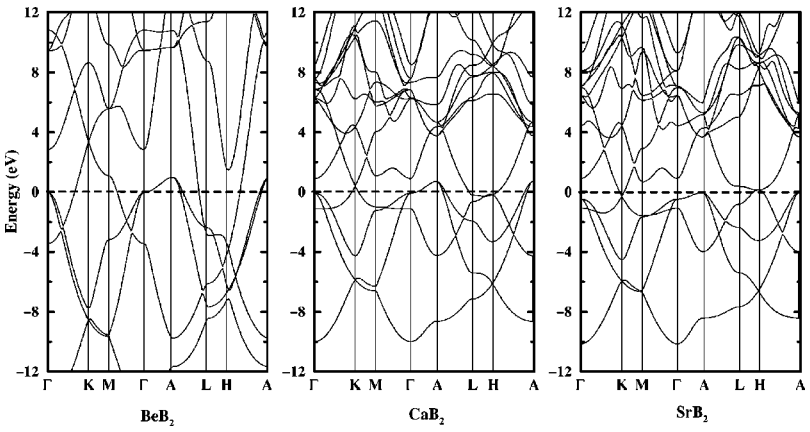


FIG. 5. The band structure of $BeB_2$, $CaB_2$, and $SrB_2$ with $AlB_2$-type structure as obtained using the optimized lattice parameters.

of VB in $CaB_2$ and $SrB_2$ have large nonbonding B $p$ states (Fig. 4). This will give a negative contribution to the one-electron eigenvalue sum for stability. This may be the reason why $CaB_2$ and $SrB_2$ are not stabilized in the $AlB_2$-type structure.

The number of valence electrons per B,C is same for LiBC and $MgB_2$. So, if electron per atom ratio is the decisive factor for the superconducting behavior of $MgB_2$ one can expect superconductivity for LiBC. Hence, we have also performed electronic band-structure studies for LiBC. The calculated DOS (Fig. 4) predicts insulating behavior with a band gap of 1.81 eV. LiBC is an indirect band-gap insulator where the band gap is between the top of VB in the $\Gamma$–$K$ direction and the bottom of CB at the $M$ point (Fig. 6). The establishment of insulating behavior is consistent with the experimental observation[42] of a very small conductivity for LiBC. The flat-band feature present in the $K$–$M$ and $\Gamma$–$A$ directions of BZ just below $E_F$ around $-0.23$ eV (Fig. 6) suggests that LiBC may be tuned to become superconducting upon hole doping.

The calculated total DOS (Fig. 4) for $MgB_2C_2$ also shows insulating behavior (which has the same number of valence electrons per nonmetal atom as $MgB_2$) with band gap of 1.04 eV. This is further confirmed by the band structure (Fig. 6), which shows indirect band-gap insulating features between the topmost valence band in the $Y$–$\Gamma$ direction and the bottom-most conduction band at the $\Gamma$ point. The interesting aspect of Fig. 6 is that there is a flat band present in the vicinity of $E_F$ (around the $\Gamma$–$Z$ and $T$–$Y$ directions) similar to that in $MgB_2$ and superconducting transition-metal borocarbides (e.g., $YNi_2B_2C$, $LuNi_2B_2C$). Consequently we suggest superconductivity with relatively high $T_c$ for hole doped $MgB_2C_2$. A more detailed analysis of the band structure shows that the narrow band in the $T$–$Y$ direction near $E_F$ is stemming from the C $p_z$ electrons. Except for the structural data[41] no other information on the physical properties of $MgB_2C_2$ is available experimentally.

If it is the boron layers that are responsible for the superconductivity, one could expect superconductivity in $MgB_4$. However, the calculated total DOS for $MgB_4$ shows (Fig. 4) only features which point toward insulating behavior and hence superconductivity is not expected for this material.

### B. EFG and NMR frequency

From the FPLAPW calculations we have estimated the electric field gradient ($V_{zz}$) at the Mg and B sites as $-0.249\times10^{21}$ and $2.047\times10^{21}$ V/m$^2$, respectively. Using the calculated $V_{zz}$ along with the nuclear quadrupole moment for $^{11}$B (0.037 b) (Ref. 60) we can calculate the NMR quadrupole coupling frequency ($\nu_q$) by means of the relation

$$\nu_q = \frac{3eQV_{zz}}{2hI(2I-1)}$$

using $I=3/2$ as the nuclear spin quantum number for $^{11}$B. This gave $\nu_q = 915$ kHz in good agreement with 828 kHz

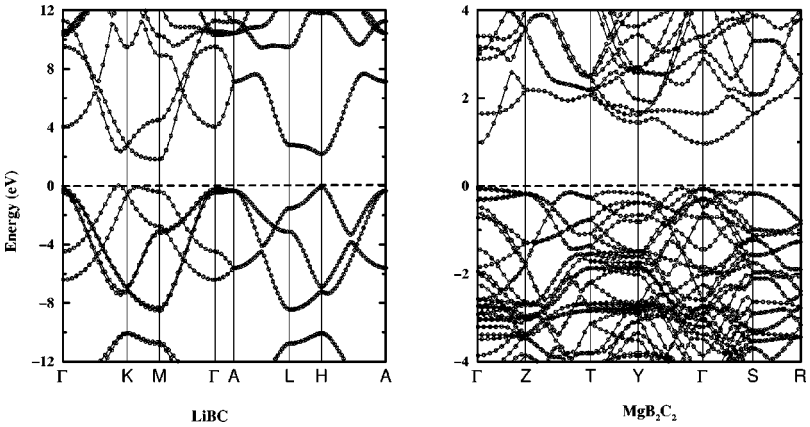


FIG. 6. The band structure of LiBC and $MgB_2C_2$ as obtained with the TBLMTO method using experimental lattice parameters.

obtained by Gerashenko *et al.*[13] and 835±5 kHz obtained by Jung *et al.*[14] from first-order quadrupole perturbed NMR spectra.

### C. Chemical bonding in $MgB_2$

Similar to the C–C distances in the graphite structure, the distance between the boron planes in $MgB_2$ is about twice the intraplanar B–B distance and hence the B–B bonding is strongly anisotropic. A more quantitative assessment of the bonding situation in $MgB_2$ can be obtained from the partial DOS (Fig. 3), which demonstrates that the B $s$ states are hybridized with the B $p$ state in VB. This shows strongly bonded $sp^2$ hybrids in the $ab$ plane. The Mg $s$ electrons contribute very little to VB and are mainly reflected in the unoccupied state. Hence Mg donates electrons to the boron layers. The B $2s$ electrons are well localized and their contribution at $E_F$ is minor. From the orbital projected DOS (Fig. 3) it is clear that B $p_x$ and $p_y$ characters are mainly dominating at $E_F$. This suggests that the $p$–$p$ $\sigma$ bonding between the boron atoms has a significant influence on superconductivity. It is worth recalling that the recently found[28] superconductor $Na_{0.29}HfNCl$ ($T_c \approx 25$ K) has N $p_x$ and $p_y$ characters at $E_F$.[61] B $p_z$ states are present in a wide energy range and dominate at the bottom of the conduction band.

The simplest way to investigate the bonding situation between two interacting atoms in a solid is to inspect the complete COHP between them, taking all valence orbitals into account. The upper panel of Fig. 3 shows COHP for the B–B and Mg–B bonds. An interesting aspect of this illustration is that VB is filled up with bonding orbitals (negative value of COHP) and the antibonding orbitals are some ~3 eV above $E_F$. Bonding-state electrons from both B–B and Mg–B bonds are found at $E_F$. The B $s$–$s$ bonding states are found mainly at the bottom of VB around −8.5 eV. The B $p$–$p$ $\sigma$ bonding states dominate at the top of the VB region around −2 eV. Note that the COHP values for the Mg–B bonds are much smaller than for the B–B bonds indicating that the B–B bond is much stronger than the Mg–B bonds consistent with the derived elastic properties (Sec. III D).

The charge-density plot for $MgB_2$ in the (110) plane (Fig. 7) shows a low electron accumulation between Mg and B as well as a very low electron population at the Mg site (much lower than for a neutral Mg atom). These findings are a clear indication of ionic bonding between Mg and B. The large electron accumulation between the B atoms and their strongly aspherical character indicates strong covalent interaction between the B atoms as also found by our examination of partial DOS and COHP. The more or less homogeneous charge distribution between the Mg atoms suggest an appreciable degree of metallic bonding between them, i.e., apart from strong ionic and covalent bonding in $MgB_2$ the band structure shows features similar to the $s$–$p$ metals. Hence, $MgB_2$ is a typical example of a mixed bonded solid.

### D. Elastic properties

Structural parameters for $BeB_2$, $CaB_2$, and $SrB_2$ are not available experimentally and we have therefore made structural optimization for these diborides along with $MgB_2$ by total energy minimization. The optimized structural parameters along with the bulk modulus, its pressure derivative, and $N(E_F)$ are given in Table I. The calculated equilibrium volume for $MgB_2$ is found to be in excellent agreement with the experimental value,[40] and the corresponding $c/a$ value is only 0.42% smaller than the experimental value. These results indicate that density-functional theory works well for this material. The calculated $N(E_F)$ value for $MgB_2$ is larger than that for the other diborides considered in the present study and this may be one of the reasons for the superconductivity in $MgB_2$.

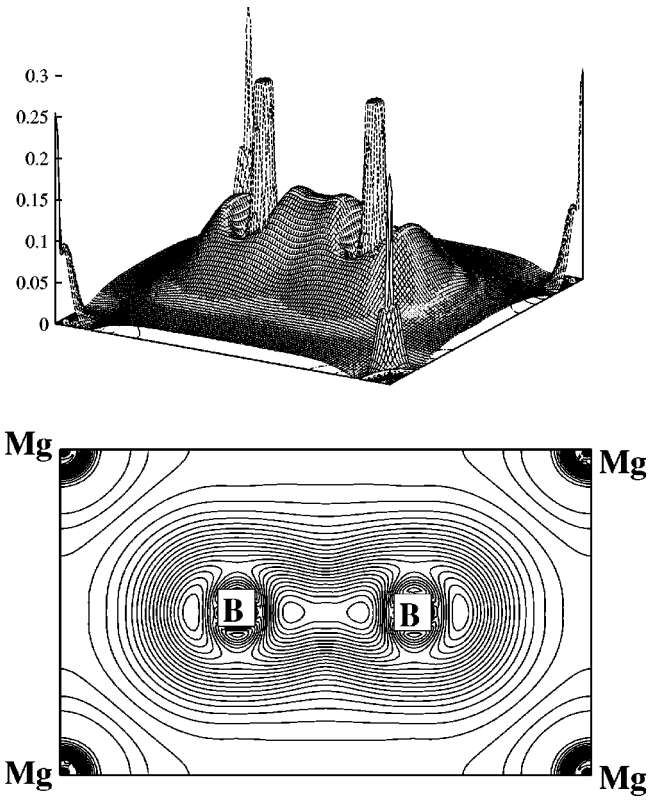


FIG. 7. Valence-charge density in the (110) plane for $MgB_2$. Corner atoms are Mg and the others are B. Both plots have 35 contours between 0 and 0.25 electrons/a.u.[3]

By fitting the total-energy versus volume curve to the universal equation of state we have obtained the bulk modulus ($B_0$) and its pressure derivative ($B_0'$) as 1.50 Mbar and 3.47, respectively. The derived $B_0$ is found to be in excellent agreement with the value 1.51 Mbar obtained from high-resolution x-ray powder diffraction measurements[33] and also in good agreement with other results listed in Table I. Furthermore $B_0 = 1.5$ Mbar obtained in this way is in good agreement with the value 1.509 Mbar estimated from the calculated single-crystal elastic constants by means of the relation

$$B = \frac{2(c_{11}+c_{12})+4c_{13}+c_{33}}{9}.$$

The electron per atom ratio of $TiB_2$ is same as that of $MgB_2$ and hence this material should also be considered. In $TiB_2$

TABLE II. The single-crystal elastic constants ($c_{ij}$ in Mbar) and bulk modulus values along *a* and *c* ($B_a$ and $B_c$ in Mbar).

| Compound | $c_{11}$ | $c_{12}$ | $c_{13}$ | $c_{33}$ | $c_{44}$ | $B_a$ | $B_c$ |
|---|---|---|---|---|---|---|---|
| $MgB_2$ | 4.380 | 0.430 | 0.329 | 2.640 | 0.802 | 5.406 | 3.006 |
| | | | | | | $4.1\pm0.2$[a] | $2.92\pm0.12$ |
| | | | | | | 6.25[b] | 3.33 |
| $TiB_2$ (expt)[c] | 6.6 | 0.48 | 0.93 | 4.32 | 2.6 | 8.512 | 5.527 |

[a]From synchrotron XRD by Prassides *et al.* (Ref. 34).
[b]From hydrostatic high-pressure synchrotron XRD by Goncharov *et al.* (Ref. 63).
[c]Derived from the single-crystal elastic constants of Spoor *et al.* (Ref. 62).

$E_F$ is located in a pseudogap and hence $N(E_F)$ is small resulting in nonobservation of superconductivity. The calculated bulk modulus for $TiB_2$ is larger than that for diborides considered in the present study. This is an effect of the filling of the bonding states in the bands and this aspect has been discussed in Ref. 59.

From various distortions we have calculated all five single-crystal elastic constants for $MgB_2$ (Table II). Unfortunately there are no experimental elastic constants available since a suitable single crystal of $MgB_2$ has so far not been obtained. We have therefore made comparison with the experimental[62] data for $TiB_2$. Despite the layered crystal structure of $MgB_2$ the high-pressure total-energy studies of Loa and Syassen[32] suggested isotropic compressibility and concluded that the intra- and interlayer bonding are of similar strength. Another high-pressure study (up to 8 GPa) by Vogt *et al.*[33] concluded that there are small anisotropies in the mechanical properties. The isothermal compressibility measurements of $MgB_2$ by synchrotron x-ray diffraction revealed[34] a stiff tightly packed incompressible nature with only moderate anisotropy between intra- and interlayer bonds. The neutron diffraction measurements by Jorgensen *et al.*[35] at high pressures concluded with highly anisotropic mechanical properties for $MgB_2$. As the experimental results are mutually inconsistent, theoretical studies of the compressibility may be helpful in resolving the ambiguities.

From the calculated single-crystal elastic constants we have derived the bulk moduli along the crystallographic directions using the relations given in Sec. II and the results are listed in Table II. The compressibility study[34] by synchrotron radiation show isothermal interlayer compressibility, $d\ln c/dP$ at zero pressure is 1.4 times the in-plane compressibility, $d\ln a/dP$. However, the high-pressure neutron diffraction studies[35] show that $d\ln c/dP=1.64\,d\ln a/dP$, which is much closer to our calculated relationship $d\ln c/dP=1.79\,d\ln a/dP$ (Table II). The most recent high-pressure measurement[63] with hydrostatic pressures up to 15 GPa shows a larger anisotropy $d\ln c/dP=1.875\,d\ln a/dP$. The larger compressibility along *c* than along *a* can be understood as follows. There is strong B $p_x,p_y$–$p_x,p_y$ covalent hybridization along *a* in $MgB_2$ and hence the bulk modulus along *a* (*b*) is large. There is significant ionic contribution to the bonding between Mg and B along *c*. Usually an ionic bond is weaker than a covalent bond and hence the bulk modulus is smaller along *c* than along *a*. The large anisotropy in the compressibility is also consistent with the fact[35] that the thermal expansion along *c* is about twice that along *a*. Moreover, substitution[16] of Al for Mg decreases *c* at a rate approximately twice that of *a* indicating the anisotropic nature of the bonding.

It is possible to visualize the anisotropy in the elastic properties from the curvature of the total energy with respect to length changes in an arbitrary direction. From the elastic compliance constants ($s_{ij}$) it is possible to derive the directional bulk modulus *K*, using the relation:[64]

$$\frac{1}{K}=(s_{11}+s_{12}+s_{13})-(s_{11}+s_{12}-s_{13}-s_{33})l_3^2, \qquad (3)$$

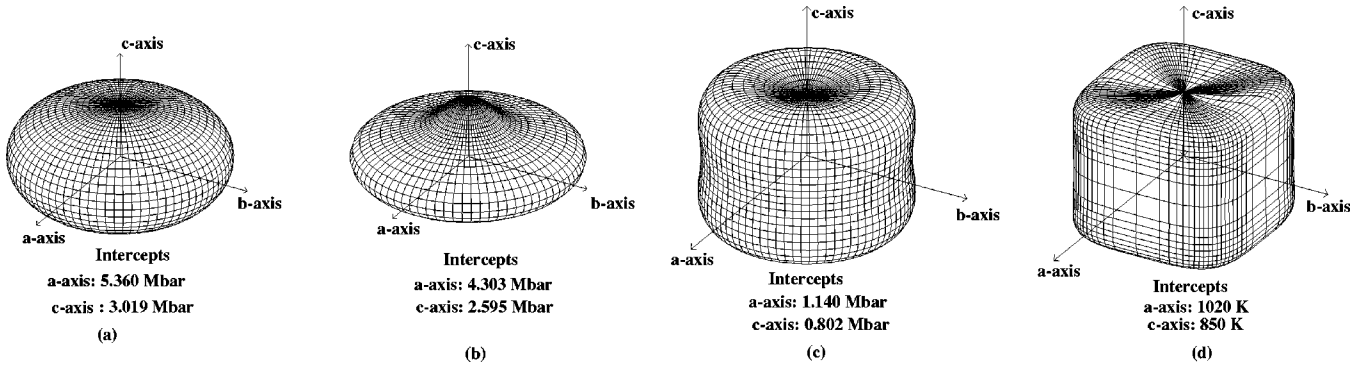


FIG. 8. Calculated directional-dependent (a) bulk, (b) Young's, (c) shear moduli, and (d) the characteristic temperature $\theta_D$ for $MgB_2$ as obtained from the calculated single-crystal elastic constants.

TABLE III. Average shear modulus ($G_{av}$ in Mbar), longitudinal and transverse elastic wave velocity ($\nu_l$, $\nu_k$ in m/s), and Debye temperature ($\theta_D$ in K) obtained from single-crystal elastic constant.

| Compound | $G_{av}$ | $\nu_l$ | $\nu_m$ | $\theta_D$ (calc) | $\theta_D$ (expt) |
|---|---|---|---|---|---|
| $MgB_2$ | 1.146 | 10 612 | 7276 | 1016 | $750\pm30$[a]<br>746[b]<br>800[c]<br>920[d] |
| $TiB_2$ (expt) [e] | 2.407 | 7 061 | 5105 | 743 | |

[a]From specific heat measurements by Bud'ko *et al.* (Ref. 10).
[b]From specific heat measurements by Wälti *et al.* (Ref. 79).
[c]From specific heat measurements by Kremer *et al.* (Ref. 85).
[d]From specific heat measurements by Wang *et al.* (Ref. 86).
[e]Derived from the single-crystal elastic constants of Spoor *et al.* (Ref. 62).

where $l_3$ is the direction cosine. The thus obtained directional-dependent bulk modulus is shown in Fig. 8(a). A useful surface construction is one that shows the directional dependence of Young's modulus ($E$), which for hexagonal symmetry can be defined as

$$\frac{1}{E}=(1-l_3^2)^2 s_{11}+l_3^4 s_{33}+l_3^2(1-l_3^2)(2s_{13}+s_{44}). \quad (4)$$

The thus derived directional-dependent Young's modulus [Fig. 8(b)] also shows large anisotropy, $E$, along $a$ being about 65% larger than along $c$. The anisotropic nature of the bonding behavior reflected in the elastic properties is consistent with the charge density analysis. The marked anisotropic compressibility of $MgB_2$ will lead to different pressure effects on different phonon modes and is also more likely to lead to pressure-induced changes in the electronic structure at $E_F$. This information is valuable in testing the predictions of competing models[5,11] for the mechanism of superconductivity.

The anisotropy in the plastic properties of materials can be studied from the directional-dependent shear stress and the amount of shear.[65] So, it is interesting to study the directional dependence of the shear in $MgB_2$. We have calculated the directional-dependent shear modulus ($G$) from the elastic constants using the relation

$$\frac{1}{G}=s_{44}+\left(s_{11}-s_{12}-\frac{s_{44}}{2}\right)(1-l_3^2)+2(s_{11}+s_{33}-2s_{13}-s_{44}) \times(1-l_3^2)l_3^2. \quad (5)$$

The directional-dependent shear modulus [Fig. 8(c)] also shows large anisotropy and $G$ along the $a$ axis is around 42% higher than that along $c$. It should be noted that large shear value is present in between the basal plane and perpendicular to it. From the calculated directional-dependent bulk modulus and the shear modulus one can calculate the directional dependence of sound velocity and hence the characteristic temperature of the material. The calculated characteristic temperature given in Fig. 8(d) shows an anisotropic nature due to the anisotropy in the bonding behavior. The calculated average shear modulus ($G_{av}$), elastic-wave velocities ($\nu$), and $\theta_D$ obtained from our single-crystal elastic constants are listed in Table III. The calculated value of $\theta_D$ is comparable with the experimental values obtained from specific heat measurements (Table III). The higher value of $\theta_D$ indicates the presence of higher phonon frequencies in this material. The existence of phonon modes at very high energies (97 meV in $MgB_2$) is experimentally identified by neutron-inelastic-scattering measurements.[15,66]

### E. Optical properties

Optical properties studies are of fundamental importance, since these involve not only the occupied and unoccupied parts of the electronic structure, but also carry information on the character of the bands. In order to elucidate the anisotropy in the optical properties of $MgB_2$ the calculated imaginary parts of dielectric tensor for $E\|a$ and $E\|c$ ob-

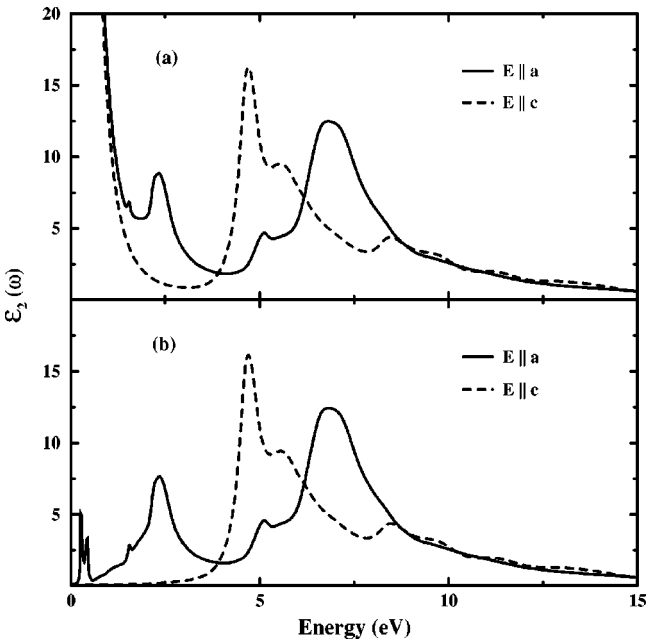


FIG. 9. The calculated optical-dielectric tensor for $MgB_2$ obtained from (a) with and (b) without intraband contribution obtained from the FPLMTO calculation.

tained from FLMTO method are shown in Fig. 9. The important feature conveyed by the interband transition shown in Fig. 9 is that there is negligible contribution to $\epsilon_2(\omega)$ in $E\|c$ below 3.8 eV. The interesting aspect for $MgB_2$ is that even though the interband contribution to the optical spectra is highly anisotropic the calculated intraband contribution show nearly isotropic behavior. This originates from the close values of the calculated plasma frequencies; 7.13 and 6.72 eV for in-plane and perpendicular-to-plane, respectively. These values are in excellent agreement with $\omega_{p,x}=7.02$ eV and $\omega_{p,z}=6.68$ eV obtained by full-potential LMTO calculation.[21] The intraband contribution to the optical dielectric tensor have been calculated similar to Ref. 52. The calculated $\epsilon_2(\omega)$ spectra which include both inter- and intraband contributions are shown in the upper panel of Fig. 9. From these $\epsilon_2(\omega)$ spectra one can derive all linear optical properties. Unfortunately, there are no experimental spectra available for $MgB_2$.

### F. Superconductivity aspects

Let us first look for similarities between $MgB_2$ and other superconducting materials. There are correlations that exist[67,68] between average electronegativity ($\eta$) and superconducting transition temperature in that the $\eta$ value is between 1.3 and 1.9 for conventional superconductors and 2.43 to 2.68 for high-$T_c$ cuprates. The $\eta$ value for $MgB_2$ is 1.733, which places this material in the category of the conventional superconductors. However, using the proposed correlation[69] between superconducting transition temperature and the value of the electronic specific heat coefficient ($\gamma$) for various superconductors we find that $\gamma$ for $MgB_2$ falls in the region of the high-$T_c$ cuprates [viz. $MgB_2$ has a low value of $N(E_F)$ as well as higher $T_c$]. In the conventional superconductors ($\beta$-W-type) with $A_3B$ composition, the mutually orthogonally permuted linear $\cdots A\text{–}A\text{–}A\cdots$ chains are believed to be responsible for the superconductivity. In $MgB_2$, the boron atoms in the zig-zag chains (Fig. 1) are believed to play an important role for the superconducting behavior. For higher $T_c$ superconducting intermetallics Butler[70] has suggested a rule of togetherness which prescribes that (for a given crystal structure, electron-per-atom ratio and period) the electron–phonon coupling is enhanced when the transition-metal atoms are brought closer together. It is interesting to note that the B atoms are brought close together by the strong covalent bonding in $MgB_2$. Earlier studies[71] show that $\beta$-ZrNCl is a semiconductor with a band gap of $\sim 3$ eV that upon Li intercalation (electron donation) becomes superconducting with $T_c=13$ K.[28] This similarity is present for $MgB_2$ also, in that the electron donation from Mg to $B_2$ leads to superconductivity. Ledbetter[72] points out that the superconducting transition temperature in high-$T_c$ cuprates increases with increasing Debye temperature ($\theta_D$). The higher $T_c$ in $MgB_2$ may be associated with the large $\theta_D$ in this material and this criterion would place $MgB_2$ together with high-$T_c$ cuprates.

In conventional superconductors, $T_c$ increases with decreasing $\theta_D$, i.e., with lattice softening.[72] The calculated $\theta_D$ for $MgB_2$ from the elastic constants is (1016 K) exceptionally large indicating that some novel mechanism is responsible for the higher $T_c$ in $MgB_2$. Using the concept that temperature-dependent electronic screening arising from narrow bands in the vicinity of $E_F$ causes temperature-dependent phonon-mode frequencies (Fig. 2), one is led to expect that softening of phonon modes does occur to explain the experimentally observed higher $T_c$. Therefore, experimental temperature-dependent phonon spectra for $MgB_2$ is required to establish whether the softening of particular phonon modes is responsible for its high $T_c$.

The superconducting transition temperature for the strongly coupled superconductors according to the McMillan formula[73] is

$$T_c=\frac{\theta_D}{1.45}\exp\left[-\frac{1.04(1+\lambda)}{\lambda-\mu^*(1+0.62\lambda)}\right]. \tag{6}$$

In Eq. (6) large $T_c$ can be obtained when we have large values for $\theta_D$ (which $MgB_2$ has) and the electron–phonon coupling constant $\lambda$. The empirical value of the Coulomb coupling constant $\mu^*$ for $sp$ metals is 0.1. The McMillan–Hopfield expression for $\lambda$ which enters in the exponent in the expression for $T_c$ is

$$\lambda=\frac{N(E_F)\langle I^2\rangle}{M\langle\omega^2\rangle}.$$

Here, $N(E_F)$ is smaller for $MgB_2$ than for conventional higher-$T_c$ materials, $\langle I^2\rangle$ is the averaged square of the electron–phonon matrix element, $\langle\omega^2\rangle$ is the averaged square of the phonon frequency, and $M$ is the mass of the ion involved. If the superconductivity occurs by phonon mediation, higher $T_c$ in $MgB_2$ can be explained as follows. Selected phonon modes may be strongly coupled to the electronic system and influence the magnitude of $T_c$ to a greater extent than average phonon modes because the average phonon mode $\langle\omega^2\rangle^{1/2}=0.69\theta_D$ is larger in $MgB_2$ (which will reduce the $\lambda$ value). Consistent with the above-mentioned viewpoint the lattice-dynamical calculations[7,21,74,75] reveal that the in-plane boron phonons near the zone center are highly anharmonic with significant nonlinear contribution to the electron–phonon coupling. If such a situation occurs, the softening of certain phonons in combination with the light mass of the constituents may lower the phonon contribution ($M\langle\omega_{\rm ph}^2\rangle$) and in turn enhance the electron–phonon coupling constant and hence $T_c$. This may explain why $MgB_2$ possesses higher $T_c$ despite the lower value of $N(E_F)$.

Now we will compare $MgB_2$ with relevant superconducting materials. Among the other transition metal diborides, superconductivity with $T_c=9.5$ K has been observed in $TaB_2$ recently.[76] Our electronic-structure studies[59] show that $E_F$ is located at a peak in the DOS profile in $TaB_2$. This feature along with the large $N(E_F)$ value of 2.92 states/(Ry f.u.) will explain the large $T_c$ in this material. As there are substantial B $p$ states at $E_F$ in $MgB_2$ similar to superconducting $RENi_2B_2C$, it may be worthwhile to compare these cases. An experimental soft x-ray emission spectroscopy study[77] on superconducting $YNi_2B_2C$ and nonsuperconduct-

ing $LaNi_2B_2C$ along with band-structure calculation[78] indicate that the superconductivity appears only when broad B $p$ bands are located at $E_F$. The main difference between the electrons involved in the transport properties of $RENi_2B_2C$ and $MgB_2$ is that the former has a remarkable DOS peak at $E_F$ dominated by Ni $3d$ states with almost equal proportions of all five Ni $3d$ states and also involves some rare-earth $d$ and B, C $s-p$ admixture whereas $MgB_2$ does not show any peak feature at $E_F$. From the accurate analysis of measured[79] specific heat over a wide temperature range $\gamma$ for $MgB_2$ is estimated as 5.5 mJ/mol $K^2$. From our calculated $N(E_F)$ value we have derived the electronic contribution to the specific-heat coefficient without electron–phonon mass enhancement yielding a value of 1.73 mJ/mol $K^2$. From this value along with the experimental $\gamma_{\text{expt}}$ we have estimated the value of the electron–phonon coupling constant using the relation $\gamma_{\text{expt}}=\gamma_{\text{th}}(1+\lambda)$ which gave $\lambda=2.17$. The large $\lambda$ value indicates that $MgB_2$ is a strongly coupled superconductor and the strong coupling as well as the low mass of B can explain the higher $T_c$ in $MgB_2$.

Using the calculated plasma frequencies in the $ab$ plane ($\Omega_{p_x,p_y}=7.13$ eV) and perpendicular to it ($\Omega_{p_z}=6.72$ eV) along with $N(E_F)=0.71$ states/(eV f.u.) the calculated Fermi velocities ($\nu_F$) using the relation

$$\nu_F=\sqrt{\frac{\Omega_p^2}{4\pi e^2 N(E_F)}}$$

are $5.15\times10^7$ and $4.85\times10^7$ cm/s along the $ab$ plane and perpendicular to it, respectively. The average Fermi velocity obtained from our calculation is $8.75\times10^7$ cm/s and this is found to be in good agreement with $8.9\times10^7$ cm/s obtained by Shulga *et al.*[80] Using the superconducting gap $\Delta=3.53k_BT_c/2=6$ meV we have calculated the coherence length ($\xi$) and the field penetration depth ($\Lambda$)

$$\xi=\frac{\hbar\nu_F}{\pi\Delta}=301\ \text{Å},\quad \Lambda=\frac{c}{\Omega_p}=282\ \text{Å}.$$

The experimental upper critical field, $H_{c2}(T)$, thermodynamic critical field, $H_c(T)$, and critical current, $J_c$, indicate that $MgB_2$ is a type-II superconductor.[81]

Now we will try to understand the effect of pressure on the superconductivity in $MgB_2$. Addition of Mg to the boron sublattice gives 15% shortening of the $c$ axis compared to that in graphite.[11] This chemical pressure brings the B semimetal to a superconducting state. As the transport properties for $MgB_2$ come from the holes, it is suggested that the superconductivity may be understood within the formalism developed for high-$T_c$ cuprates.[5] This predicts a positive pressure coefficient for $T_c$ as a result of the decreasing intraplane B–B distance with increasing pressure. However, $T_c$ is experimentally[31] found to decrease with pressure at a rate of $-1.11$ K/GPa. The RVB theory,[11] on the other hand, predicts a decrease in $T_c$ with increasing chemical pressure, consistent with the experimental findings.[31,82,83] Linear response calculations[21] show that the B-bond stretching modes have unusually strong coupling to electrons close to $E_F$ at the top of the bonding quasi-two-dimensional B $\sigma$ bonds. Therefore, when the compressibility is larger within the $ab$ plane than along $c$, one can expect a large variation in the superconductivity with pressure (because the flat bands with $p_x,p_y$ characters broaden faster by compression). Our calculated elastic property for $MgB_2$ shows large anisotropy with easy compression along $c$. Hence, the key energy band (which is sensitive to the B-bond stretching) will broaden slowly with pressure and $T_c$ will slowly decrease with increasing pressure, consistent with experimental results.

## IV. SUMMARY

The present study shows a common origin between the superconductivity in rare earth transition metal borocarbides and $MgB_2$ in that there is a flat band present in the vicinity of the Fermi level and also that the B atoms are primarily involved in electron–phonon coupling in these materials. Owing to the lack of single crystals the anisotropy in physical properties of $MgB_2$ are not studied experimentally. We predicted large anisotropies in the optical and mechanical properties. From detailed electronic-structure studies we have arrived at the following conclusions.

(1) The bonding behavior of $MgB_2$ has been explained by analyses of site-, angular momentum-, and orbital-projected density of states as well as charge-density and crystal-overlap Hamiltonian population. These analyses establish a mixed-bonding behavior with ionic bonding between Mg and B, covalent bonding between B atoms, and metallic bonding between Mg and Mg like that in $sp$ metals.

(2) We identified a large anisotropy in the mechanical properties of $MgB_2$ from our calculated elastic constants, consistent with the anisotropy in the bonding behavior and high-pressure neutron-diffraction measurements. Consequently, pressure can influence the bands in different directions of BZ in an unusually different manner and hence the physical properties.

(3) Two degenerate flat bands have been identified near $E_F$ in the $\Gamma-A$ direction of BZ. These degenerate B $p_x,p_y$ bands are considered as the key to the realization of the high superconducting temperature in $MgB_2$.

(4) The role of Mg in $MgB_2$ is to donate electrons to the B atoms and hence to shift $E_F$ such that it lies very close to the flat band, the feature which we believe to be important for superconductivity.

(5) We found similarity in the electronic structures of $MgB_2$, LiBC, and $MgB_2C_2$. Therefore superconductivity is expected in hole doped $MgB_2C_2$ and LiBC. On the other hand, the electronic structures of $BeB_2$, $CaB_2$, $SrB_2$, and $MgB_4$ suggest a low probability for superconductivity.

(6) Because of the nearly flat bands in the vicinity of $E_F$ (which will introduce temperature-dependent electronic screening of the phonon-mode frequencies), we expect temperature-dependent phonon-mode softening or large anisotropy in the phonon modes.

(7) The calculated boron NMR frequency is found to be in very good agreement with the experimental studies.

(8) As our calculated Debye temperature for $MgB_2$ is much larger than for other superconducting intermetallics,

we believe that selected phonon modes can be strongly coupled to the electronic system and thus influence the magnitude of $T_c$ to a greater extent than the average phonon correlations may indicate.

(9) If the rigid-band-filling approximation works and also the electrons are responsible for the superconductivity of $MgB_2$, our calculation suggests that a doping by 0.32 electrons will enhance $T_c$. However, the experimental observation of a reduction in $T_c$ by electron doping of $MgB_2$ indicates that the holes are responsible for the superconductivity.

**ACKNOWLEDGMENTS**

P.R. is grateful for financial support from the Research Council of Norway. Part of these calculations was carried out on the Norwegian supercomputer facilities (Program for Supercomputing). P.R. wishes to acknowledge Professor O.K. Andersen, Professor Ove Jepsen, Dr. Florent Boucher, Dr. John Wills, Professor K. Schwarz, and Professor Peter Blaha for providing some of the programs used in this study, and Dr. Anna Delin and Dr. Lars Fast for useful communications.

*Electronic address: ravindran.ponniah@kjemi.uio.no

[1] J. Nagamatsu, N. Nakagawa, T. Muranaka, Y. Zenitani, and J. Akimitsu, Nature (London) **410**, 63 (2001).

[2] J.G. Bednorz and K.A. Müller, Z. Phys. B: Condens. Matter **64**, 189 (1986).

[3] L. Gao, Y.Y. Xue, F. Chen, Q. Xiong, R.L. Meng, D. Ramirez, C.W. Chu, J.H. Eggert, and H.K. Mao, Phys. Rev. B **50**, 4260 (1994).

[4] J. Kortus, I.I. Mazin, K.D. Belashchenko, A.P. Antropov, and L.L. Boyer, cond-mat/0101446 (unpublished).

[5] J.E. Hirsch, cond-mat/0102115 (unpublished).

[6] K.D. Belashchenko, M. van Schilfgaarde, and V.P. Antropov, cond-mat/0102290 (unpublished).

[7] J.M. An and W.E. Pickett, cond-mat/0102391 (unpublished).

[8] W.N. Kang, C.U. Jung, K.H.P. Kim, M.S. Park, S.Y. Lee, H.J. Kim, E.M. Choi, K.H. Kim, M.S. Kim, and S.L. Lee, cond-mat/0102313 (unpublished).

[9] A.K. Gangopadhyay, A.J. Schwetz, and J.S. Schilling, Physica C **246**, 317 (1995).

[10] S.L. Bud'ko, G. Lapertot, C. Petrovic, C.E. Cunningham, N. Anderson, and P.C. Canfield, Phys. Rev. Lett. **86**, 1877 (2001).

[11] G. Baskaran, cond-mat/0103308 (unpublished).

[12] H. Kotegawa, K. Ishida, Y. Kitaoka, T. Muranaka, and J. Akimitsu, cond-mat/0102334 (unpublished).

[13] A. Gerashenko, K. Mikhalev, S. Verkhovskii, T. D'yachkova, A. Tyntynnik, and V. Zubkov, cond-mat/0102421 (unpublished).

[14] J.K. Jung, S.H. Baek, F. Borsa, S.L. Bud'ko, G. Lapertot, and P.C. Canfield, cond-mat/0103040 (unpublished).

[15] T.J. Sato, K. Shibata, and Y. Takano, cond-mat/0102468 (unpublished).

[16] J.S. Slusky, N. Rogado, K.A. Regan, M.A. Hayward, P. Khalifah, T. He, K. Inumaru, S. Loureiro, M.K. Haas, H.W. Zandbergen, and R.J. Cava, cond-mat/0102262 (unpublished).

[17] J.S. Ahn and E.J. Choi, cond-mat/0103169 (unpublished).

[18] T. Takenobu, T. Ito, D.H. Chi, K. Prassides, and Y. Iwasa, cond-mat/0103241 (unpublished).

[19] W.N. Kang, C.U. Jung, K.H.P. Kim, M.S. Park, S.Y. Lee, H.J. Kim, E.M. Choi, K.H. Kim, M.S. Kim, and S.I. Lee, cond-mat/0102313 (unpublished).

[20] C. Panagopoulos, B.D. Rainford, T. Xiang, C.A. Scott, M. Kambara, and I.H. Inoue, cond-mat/0103060 (unpublished).

[21] Y. Kong, O.V. Dolgov, O. Jepsen, and O.K. Andersen, cond-mat/0102499 (unpublished).

[22] R. Nagarajan, C. Mazumdar, Z. Hossain, S.K. Dhar, K.V. Gopalakrishnan, L.C. Gupta, C. Godart, B.D. Padalia, and R. Vijayaraghavan, Phys. Rev. Lett. **72**, 274 (1994).

[23] R.J. Cava, K. Takaki, B. Batlogg, H.W. Zandbergen, J.J. Krajewski, W.F. Peck, Jr., R.B. van Dover, R.J. Felder, T. Siegrist, K. Mizuhahi, J.O. Lee, H. Elsaki, S.A. Carter, and S. Uchida, Nature (London) **367**, 146 (1994); R.J. Cava, H. Takagi, H.W. Zandbergen, J.J. Krajewski, W.F. Peck, Jr., T. Siegrist, B. Batlogg, R.B. van Dover, R.J. Felder, K. Mizuhashi, J.O. Lee, H. Eisaki, and S. Uchida, *ibid.* **367**, 252 (1994).

[24] R.J. Cava, H.W. Zandbergen, B. Batlogg, H. Eisaki, H. Tagaki, J.J. Krajewski, W.F. Peck, Jr., E.M. Gyorgy, and S. Uchida, Nature (London) **372**, 245 (1994); H.W. Zandbergen, J. Jansen, R.J. Cava, J.J. Krajewski, and W.F. Peck, Jr., *ibid.* **372**, 759 (1994).

[25] A.D. Chinchure, R. Nagarajan, and L.C. Gupta, Physica B **281&282**, 894 (2000).

[26] J. C. Philips, *Physics of High-$T_c$ Superconductors* (Academic, New York, 1989).

[27] K. P. Sinha and S. L. Kakani, *Magnetic Superconductors* (Nova Science, Commack, 1989).

[28] S. Yamanaka, H. Kawaji, K. Hotehama, and M. Ohashi, Adv. Mater. **9**, 771 (1996); S. Yamanaka, K. Hotehama, and H. Kawaji, Nature (London) **392**, 580 (1998).

[29] R.K. Kremer, K. Ahn, R.W. Henn, J.J. Mattausch, W. Schndle, A. Stolovits, and A. Simon, Physica C **317&318**, 456 (1999).

[30] S. Sanfilippo, H. Elsinger, M. Nunez-Regueiro, O. Laborde, S. Lefloch, M. Affronte, G.L. Olcese, and A. Palenzona, Phys. Rev. B **61**, R3800 (2000).

[31] T. Tomita, J.J. Hamlin, J.S. Shilling, D.G. Hinks, and J.D. Jorgensen, cond-mat/0103538 (unpublished).

[32] I. Loa and K. Syassen, Solid State Commun. (to be published).

[33] T. Vogt, G. Schneider, J.A. Hriljac, G. Yang, and J.S. Abell, cond-mat/0102480 (unpublished).

[34] K. Prassides, Y. Iwasa, T. Ito, D.H. Chi, K. Uehara, E. Nishibori, M. Takata, S. Sakata, Y. Ohishi, O. Shimomura, T. Muranaka, and J. Akimitsus, cond-mat/0102507 (unpublished).

[35] J.D. Jorgensen, D.G. Hinks, and S. Short, cond-mat/0103069 (unpublished).

[36] I. Felner, cond-mat/0102508 (unpublished).

[37] S.M. Kazakov, M. Angst, and J. Karpinski, cond-mat/0103350 (unpublished).

[38] Y.G. Zhao, X.P. Zhang, P.T. Qiao, H.T. Zhang, S.L. Jia, B.S. Cao, M.H. Zhu, Z.H. Han, X.L. Wang, and B.L. Gu, cond-mat/0103077 (unpublished).

[39] N.I. Medvedeva, A.L. Ivanovskii, J.E. Medvedeva, and A.J. Freeman, cond-mat/0103157 (unpublished).

[40] M.E. Jones and R.E. Marsh, J. Am. Chem. Soc. **76**, 1434 (1954).

[41] M. Wörle and R. Nesper, J. Alloys Compd. **216**, 75 (1994).

[42] M. Wörle, R. Nesper, G. Mair, M. Schwarz, and H.G. von Schnering, Z. Anorg. Allg. Chem. **621**, 1153 (1995).

[43] A. Vegas, L.A. Martinez-Cruz, A. Ramos-Gallardo, and A.

Romero, Z. Kristallogr. **210**, 575 (1995).
[44] P. Blaha, K. Schwarz, and J. Luitz, WIEN97, Vienna University of Technology, 1997 [improved and updated Unix version of the original copyrighted WIEN code, which was published by P. Blaha, K. Schwarz, P. Sorantin, and S. B. Trickey, Comput. Phys. Commun. **59**, 399 (1990)].
[45] J.P. Perdew, K. Burke, and M. Ernzerhof, Phys. Rev. Lett. **77**, 3865 (1996).
[46] O.K. Andersen and O. Jepsen, Phys. Rev. Lett. **53**, 2571 (1984).
[47] R. Dronskowski and P.E. Blochl, J. Phys. Chem. **92**, 5397 (1993).
[48] G. Krier, O. Jepsen, A. Burkhardt, and O. K. Andersen, *Tight binding* LMTO-ASA *Program Version 4.7*, Stuttgart, Germany, 1999.
[49] J. M. Wills, O. Eriksson, M. Alouani, and D. L. Price, in *Electronic Structure and Physical Properties of Solids*, edited by H. Dreysse (Springer, Berlin, 2000), p. 148; J.M. Wills and B.R. Cooper, Phys. Rev. B **36**, 3809 (1987); D.L. Price and B.R. Cooper, *ibid.* **39**, 4945 (1989).
[50] O.K. Andersen, Phys. Rev. B **12**, 3060 (1975).
[51] M. Alouani and J.M. Wills, Phys. Rev. B **54**, 2480 (1996); R. Ahuja, S. Auluck, J.M. Wills, M. Alouani, B. Johansson, and O. Eriksson, *ibid.* **55**, 4999 (1997).
[52] P. Ravindran, A. Delin, B. Johansson, O. Eriksson, and J.M. Wills, Phys. Rev. B **59**, 1776 (1999).
[53] P. Ravindran, L. Fast, P.A. Korzhavyi, B. Johansson, J. Wills, and O. Eriksson, J. Appl. Phys. **84**, 4891 (1998).
[54] D. C. Wallace, *Thermodynamics of Crystals* (Wiley, New York, 1972).
[55] P. Ravindran and R. Asokamani, J. Phys.: Condens. Matter **7**, 1 (1995).
[56] I.I. Tupitsyn, I.I. Lyakhovskaya, M.S. Nakhmanson, and A.S. Sukhikh, Sov. Phys. Solid State **16**, 2015 (1975).
[57] G. Satta, G. Profeta, F. Bernardini, A. Continenza, and S. Massidda, cond-mat/0102358 (unpublished).
[58] P. Ravindran, G. Subramoniam, and R. Asokamani, Phys. Rev. B **53**, 1129 (1996).
[59] P. Vajeeston, P. Ravindran, C. Ravi, and R. Asokamani, Phys. Rev. B **63**, 045115 (2001).
[60] V. S. Shirley and C. M. Lederer, in *Hyperfine Interactions Studied in Nuclear Reactions and Decay*, edited by E. Karlsson and R. Wäppling (Almqvist and Wiksell International, Stockholm, Sweden, 1975).
[61] R. Weht, A. Filippetti, and W.E. Pickett, Europhys. Lett. **48**, 320 (1999).
[62] P.S. Spoor, J.D. Maynard, M.J. Pan, D.J. Green, J.R. Hellmann, and T. Tanaka, Appl. Phys. Lett. **70**, 1959 (1997).
[63] A.F. Goncharov, V.V. Struzhkin, E. Gregoryanz, J. Hu, R.J. Hemley, H.K. Mao, G. Papertot, S.L. Bud'ko, and P.C. Canfield, cond-mat/0104042 (unpublished).
[64] J. F. Nye, *Physical Properties of Crystals* (Oxford University Press, Oxford, 1985).
[65] W. Boas and F. K. Mackenzie, in *Progress in Metal Physics*, edited by B. Chamers (Wiley, New York, 1968), Vol. 2, p. 90.
[66] R. Osborn, E.A. Goremychkin, A.I. Kolesnikov, and D.G. Hinks, cond-mat/0103064 (unpublished).
[67] R. Asokamani and R. Manjula, Phys. Rev. B **39**, 4217 (1989).
[68] S. Nishimoto, M. Takahashi, and Y. Ohta, Physica B **281&282**, 953 (2000).
[69] H. Takaki, R.J. Cava, H. Eisaki, J.O. Lee, K. Mizuhashi, B. Batlogg, S. Uchida, J. Jikrajewski, and W.F. Peck, Jr., Physica C **228**, 389 (1994).
[70] W. H. Butler, *Treaties on Materials Science and Technology*, edited by F. Y. Fradin (Academic, New York, 1981), Vol. 21, p. 165.
[71] M. Ohashi, S. Yamanaka, and M. Hattori, J. Ceram. Soc. Jpn. **97**, 1175 (1989).
[72] H. Ledbetter, Physica C **235-240**, 1325 (1994).
[73] W.L. Mcmillan, Phys. Rev. **167**, 331 (1967).
[74] T. Yildirim, O. Gülseren, J.W. Lynn, C.M. Brown, T.J. Udovic, H.Z. Qing, N. Rogado, K.A. Regan, M.A. Hayward, J.S. Slusky, T. He, M.K. Haas, P. Khalifah, K. Inumaru, and R.J. Cava, cond-mat/0103469 (unpublished).
[75] A.Y. Liu, I.I. Mazin, and J. Kortus, cond-mat/0103570 (unpublished).
[76] D. Kaczorowski, A.J. Zaleski, O.J. Zogal, and J. Klamut, cond-mat/0103571 (unpublished).
[77] S. Shin, A. Agui, M. Watanabe, M. Fujisawa, Y. Tazuka, T. Ishii, K. Kobayashi, A. Fujimori, M. Hinomaru, and H. Takagi, Phys. Rev. B **52**, 15 082 (1995).
[78] L.M. Mattheiss, T. Siegrist, and R.J. Cava, Solid State Commun. **91**, 587 (1994).
[79] Ch. Walti, E. Felder, C. Degen, G. Wigger, R. Monnier, B. Delley, and H.R. Ott, cond-mat/0102522 (unpublished).
[80] S.V. Shulga, S.L. Drechsler, H. Eschrig, H. Rosner, and W. Pickett, cond-mat/0103154 (unpublished).
[81] D.K. Finnemore, J.E. Ostenson, S.L. Bud'ko, V.P. Antropov, and L.L. Boyer, cond-mat/0102114 (unpublished).
[82] B. Lorenz, R.L. Meng, and C.W. Chu, cond-mat/0102264 (unpublished).
[83] E. Saito, T. Taknenobu, T. Ito, Y. Iwasa, K. Prassides, and T. Arima, J. Phys.: Condens. Matter **13**, L267 (2001).
[84] K.P. Bohnen, R. Heid, and B. Renker, cond-mat/0103319 (unpublished).
[85] R.K. Kremer, B.J. Gibson, and K. Ahn, cond-mat/0102432 (unpublished).
[86] Y. Wang, T. Plackowski, and A. Junod, cond-mat/0103210 (unpublished).